# ENHANCEMENT OF POWER FACTOR CORRECTION IN AN AC-DC CONVERTER WITH AN INTEGRATED BOOST-FLYBACK CIRCUIT

ANTO SHEEBA JOSEPH[1], SEYEZHAI RAMALINGAM[2]

**Due to advancements in semiconductor technology, modern controllers, and nonlinear characteristics, loads are increasingly used in industrial applications. Because of nonlinear traits, harmonics are introduced in the main supply, and the supply current is distorted. Numerous power factor correction (PFC) converter topologies are established for proper wave shaping. The integration of conventional PFC converters produces superior results in high voltage on the output side and improves efficiency. A single-stage boost flyback integrated PFC converter is investigated in this paper, which provides high efficiency, high output voltage, and less voltage stress. This converter uses a lesser number of components, which results in a compact size and low cost. The enhancement of power factor, efficiency, and wave shaping of the current waveform is realized through various control techniques. A novel current sensorless control for the integrated topology is investigated, and it is shown that it provides better total harmonic distortion and current wave shaping than other control techniques. A 48 W, 12/48 V prototype model is implemented to validate the simulation results practically.**

## 1. INTRODUCTION

Due to the growing pressure on global energy usage and the fact that lighting consumes most of the electrical energy, the adoption of powerful and energy-efficient light bulbs, like Light-emitting diodes (LEDs), is prioritized [1]. When LEDs are used for lighting applications, they need energy from a universal ac power source; harmonic currents are introduced into the utility. Due to this, increased applicability of mandatory harmonic reduction standards (IEC 61000-3-2 and IEEE STD 519) is introduced for power factor adjustment [2]. As LEDs need a low-voltage dc power supply, an LED lamp driver is used, which requires the ac-dc converters to act as a driver circuit [3]. Several ac-dc converter topologies are available as driver circuits for LED lighting applications [4-6]. A power factor correction (PFC) converter can help minimize power losses and lessen the incidence of harmonics, resulting in a more efficient and dependable power supply. The literature [7–10] has offered numerous PFC converter topologies and control strategies. The passive PFC approach offers a reliable solution, but its greater weight and volume result in lower power packing density. On the other hand, active PFC uses semiconductor switches to provide a more effective solution that overcomes the inability of passive PFC [11].

The active PFC is of two types: two- and one-stage converters. The most recognizable strategy is the two-stage method. A two-stage converter uses a pre-stage and post-stage dc-dc converter to correct the power factor and get the input current and voltage close to one another [12]. Components count, increased equipment complexity, and reduced system efficiency are the major disadvantages of the two-stage technique. In small power approaches like computers' power source, domestic appliances, and electronic load for discharge lamps, these disadvantages are undesirable in two-stage PFC [13,14]. The drawbacks can be avoided by using a single-stage converter, which combines the two processes. The advantages of single-stage PFC are reduced size, cost, and component count. Several single-stage converters are commonly used in power electronics, including Boost converters, Buck converters, Forward converters, flyback converters, SEPIC converters, and cuk converters [15]. These converters can be used for low-rating applications, providing higher THD and lower power factor. Many combined PFC converters with dc/dc stages have been offered as a solution in recent years. In [16], an integrated PFC converter typically employs a common dynamic switch that is common between the power factor correction stage and the dc-to-dc converter stage. [17] discusses an integrated buck-flyback converter, which avoids voltage and current surges on the main switch while the buck converter executes the purpose of PFC and controls lamp output. Examination of a single-stage Integrated Forward-flyback converter in [18] shows that this method can produce a great power factor in power electronics systems.

While the converter operates in an open-loop arrangement, the input current and voltage may be out of phase. This can result in high total harmonic distortion (THD) levels, decreased power factor, and ripple in resultant voltage. To waveshape, supply current like supply voltage, and to achieve a greater power factor and lower THD, many closed-loop control strategies are involved [19]. Linear control techniques PI/PID controllers have been used in the past, but they have challenges in tracking time-changing reference oscillations [19–21]. Various control techniques are involved to provide a better waveshape of input current.

This part of the work describes and evaluates an integrated PFC converter designed specifically for LED lighting applications. It utilizes a boost flyback topology to convert ac to dc in a single stage. To verify the theory research, a 48 W, 12/48 V boost-flyback integrated converter is built. Closed-loop techniques control the output voltage for integrated boost flyback, and comparisons are made.

## 2. DESCRIPTION OF BOOST-FLYBACK INTEGRATED CONVERTER

The reference [22] boosts its voltage gain but calls for an extensive duty cycle, increasing circuit design complexity and expense. The duty cycle D is defined as the duration of the active period within one cycle. At a high-duty cycle, the converter efficiency will be degraded. Reference [23] can produce high voltage; however, because of the transformer winding's leakage inductance, its high voltage and current may harm the switch. These disadvantages can be overcome by the boost flyback integrated converter, which offers high voltage gain at 50% duty cycle and avoids high voltage and current stress on the switch.

[1] Rajalakshmi Engineering College, Thandalam Chennai, India. E-mail: antosheeba.j@rajalakshmi.edu.in
[2] Sri Sivasubramaniya Nadar College of Engineering, Kalavakkam Chennai, India. E-mail:seyezhair@ssn.edu.in

## 2.1. BOOST-FLYBACK INTEGRATED CONVERTER CIRCUIT DESCRIPTION

Figure 1 depicts the circuit schematic for a boost-flyback integrated converter. This investigation aims to analyze a boost-flyback integrated converter and assess how well it obtains high voltage gain while minimizing output voltage ripple. The suggested converter boosts voltage gain by adding a linked inductor to a boost cell and altering its turn ratio [24].
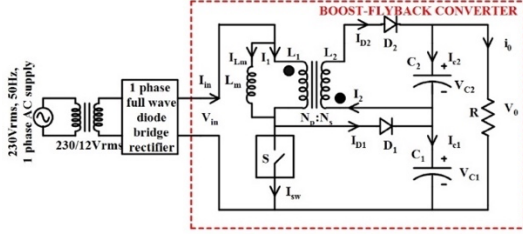


Fig. 1 – Boost-Flyback integrated PFC converter.

The boost-flyback integrated converter, unlike a standard boost converter, has a supplementary linked inductor, conversion diode, and filter capacitor. A magnetizing inductor $L_m$ and a standard transformer with a winding ratio of $N_2/N_1$ can replicate the coupled inductor. The boost output across capacitor $C_1$ and flyback output across capacitor $C_2$ are connected in series, and this design may produce an output voltage higher than that of a typical boost converter.

## 2.2. MODES OF OPERATION

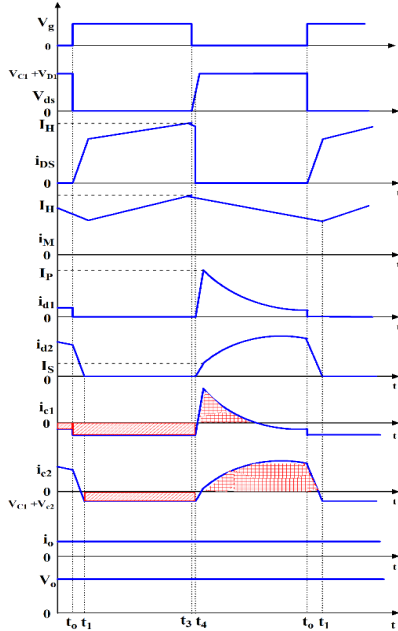Figure 2 shows the switching waveform of the boost flyback integrated converter.



Fig. 2 – Switching waveform.

During mode 1 [$t_0$–$t_1$], the switch S is activated at time zero (t0), Vin is voltage all over the magnetizing inductance, and the magnetizing current's growth curve is VLm/Lm. The diodes D1 and D2 will not conduct during this mode as they are in reverse conduction mode. Also, $C_1$ and $C_2$ deliver power to the load.

During mode 2 [$t_1$–$t_2$], diodes $D_1$ and $D_2$ undergo reverse biasing. Output capacitors $C_1$ and $C_2$ deliver energy to the load. The magnetizing current is maximum at point time $t_2$ while switch S is still turned on.

During mode 3 [$t_2$–$t_3$], when the diode $D_1$ begins to operate, a considerable amount of the $I_{Lm}$ will flow into the capacitor $C_1$ of the active clamp. This happens because of the outflow of the inductance in the outer loop. As a result, current id1 keeps dropping while $i_{d2}$ keeps rising. The current charge and discharge from $C_1$ and $C_2$ during this interval are shown as the shaded area in the $i_{C1}$ and $i_{C2}$ current waveforms.

During mode 4 [$t_3$–$t_0$], the exciting current $i_{d1}$ is forced to stream mostly into capacitor $C_1$ once diodes $D_1$ and $D_2$ begin to conduct. The secondary winding's current $i_{d2}$ progressively rises to supply the load side.

## 2.3. DESIGN OF BOOST FLYBACK INTEGRATED CONVERTER

The equations below can be derived when the primary switch S is turned on.

$$V_{in} = V_{L1} = V_{Lm}, \tag{1}$$

$$I_{C1(on)} = I_{C2(on)} = \frac{-V_0}{R} = -I_0, \tag{2}$$

$$V_0 = V_{C1} + V_{C2}. \tag{3}$$

The equations below can be derived when the primary switch S is turned off.

$$I_{C1(off)} = I_1 - \frac{V_0}{R} \text{ and } I_{C2(off)} = I_2 - \frac{V_0}{R}, \tag{4}$$

$$V_{C1} = \frac{V_{in}}{1-D} \text{ and } V_{C1} = \frac{N_2}{N_1}\left(\frac{D}{1-D}\right) V_{in}, \tag{5}$$

$$I_1 = I_{in} - \left(\frac{N_2}{N_1}\right) I_2, \tag{6}$$

$$V_{in} = V_{L1} + V_{D1} + V_{D2} + V_{L2} + V_0. \tag{7}$$

The winding ratio of the transformer is

$$\frac{N_2}{N_1} = \frac{V_{L1}}{V_{L2}}, \tag{8}$$

therefore,

$$V_{L1} = \frac{1}{1+\frac{N_2}{N_1}} (V_{in} - V_{D1} - V_{D2} - V_0). \tag{9}$$

$C_1$ and $C_2$'s average capacitor currents will be zero in a steady state condition. The volt-second balancing equation can be found using (2) and (4) depending on the condition of the steady state of capacitor $C_1$.

$$-\frac{V_0}{R}DT_s + \left(I_1 - \frac{V_0}{R}\right)(1-D)T_s = 0, \tag{10}$$

$$I_1 = \frac{V_0}{(1-D)R}. \tag{11}$$

The volt-second balancing equation can be derived from (2) and (4) under the steady-state condition of capacitor $C_2$.

$$-\frac{V_0}{R}DT_s + \left(I_2 - \frac{V_0}{R}\right)(1-D)T_s = 0, \tag{12}$$

$$I_2 = \frac{V_0}{(1-D)R}. \tag{13}$$

In the steady state, the following equation is derived from eq. (2) and (4) using the inductor volt-second balance principle

$$(V_{in} - I_{in})DT_s + \frac{1}{1+\frac{N_2}{N_1}}\binom{V_{in} - V_0 - V_{D1} - V_{D2}}{-I_2 - I_1(1-D)T_s} = 0, \tag{14}$$

$$\frac{V_0}{V_{in}} = \frac{1+D\frac{N_2}{N_1}}{1-D}. \tag{15}$$

The above equation is the converter's optimal voltage gain. Increasing the linked inductor's turns ratio and maintaining a small duty ratio result in a significant output voltage gain. The PFC converter's input supply power and output load power are feasibly obtained as

$$P_{in} = \left(1+\frac{N_2}{N_1}D\right) V_{in}I_1, \tag{16}$$

$$P_{out} = (1-D)V_0I_1. \tag{7}$$

Using eq. (16) and (17), the boost-flyback converter efficiency is calculated as

$$\eta = \frac{P_{out}}{P_{in}} = \frac{(1-D)V_0}{\left(1+\frac{N_2}{N_1}D\right)V_{in}}. \tag{18}$$

The continuous current is run through the magnetic inductance to reduce output ripple and output filter range. To make this possible, the critical magnetizing inductance and output capacitance are calculated as,

$$L_{critical} = \frac{(1-D)^2 R_L D T_s}{2\left(1+\frac{N_2}{N_1}D\right)^2}, \tag{19}$$

$$C > \frac{DI_0 T_s}{\Delta V_0}. \tag{20}$$

where $\Delta V_0$ is the output voltage ripple. The multi-flyback converters are connected in series when a larger output voltage is required.

### 2.4. SIMULATION PARAMETERS

The output voltage ripple $\Delta V_0$ is chosen as 2 V. The turns ratio should be selected to give the converter a fair duty cycle and lower the voltage impact on $C_2$ and $D_2$ to an acceptable level. As a result, n = 2 is used in this design. From eq (15), the duty cycle and D = 0.5.

Using eq. (19) and (20), the critical magnetizing inductance and output capacitor value are calculated and obtained as $L_{m,crit} = 30\mu H$, and C = 10 μF. For CCM operation, the $L_m$ values should be greater than $L_{m,critical}$. Therefore, $L_m$ is chosen as 2 mH and C = 10 μF. This serves as the necessary minimum capacitance to meet the output ripple specification. The combined capacitance of the output capacitors $C_1$ and $C_2$ must be higher than this required minimum capacitance. Table 1 shows the simulation parameters of the boost-flyback converter.

*Table 1*

Simulation parameter of boost-flyback converter

| Parameters | Values |
| --- | --- |
| Rated output power | 48 W |
| Input voltage | 12 V |
| Regulated output voltage | 48 V |
| Duty cycle | 0.5 |
| Switching frequency | 25KHz |
| Turns ratio | 2 |
| Output capacitor | 10 μ F |
| Output resistor | 48 Ω |
| Magnetizing Inductance | 2 mH |

### 2.4. BOOST FLYBACK CONVERTER SIMULATION RESULTS

Figure 3 shows the waveforms of the boost-flyback converter.
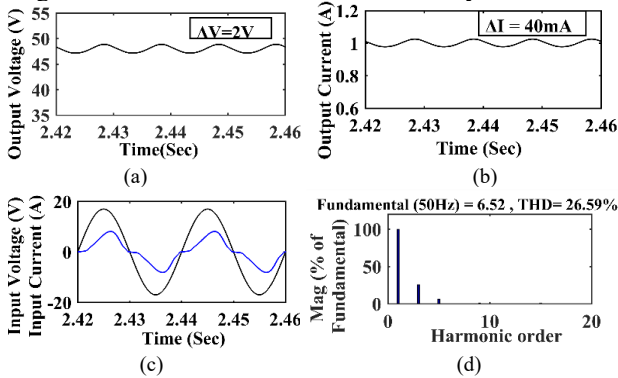


(a)

(b)

(c)

(d)

Fig. 3 – Waveforms of boost flyback integrated PFC converter: (a) load voltage with 2V ripple; (b) load current with 40mA ripple; (c) source voltage and current at constant load, (d) FFT analysis of boost flyback integrated PFC converter with THD 26.59 %

Figure 3 (a-b) shows the load voltage ripple is 2 V, and the current ripple is 40 mA. Figure 3(c) presents the open loop boost-flyback converter's simulated source voltage and source current. Figure 3d presents the THD of the boost-flyback integrated converter as 26.59 %.

## 3. SIMULATION OF AVERAGE AND CURRENT PROGRAMMED CONTROL TECHNIQUES

In most cases, the output voltage of converters is controlled by either of the two control techniques: voltage-mode control or current-mode control. Contrarily, supply current can be shaped using management techniques to reduce harmonic distortion, improving the power factor.

### 3.1 AVERAGE CURRENT MODE CONTROL TECHNIQUE

The "average current mode control" method may be a prime strategy for managing the current from the supply waveform in an extremely low harmonic converter. An electrical current waveform of exceptional quality can be produced using this method for a wide variety of supplied voltages in either uninterrupted or interrupted conduction modes. It is merely a method for controlling two loops at the same time. On the inside and outside are current and voltage loops [25]. Figure 4 represents the circuit diagram of the average current control boost-flyback integrated converter.
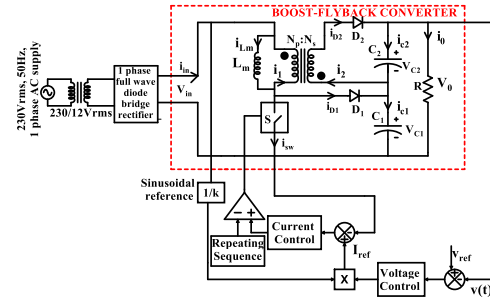


Fig. 4 – Average current control boost flyback integrated PFC converter.

The ramp pattern is compared to the output of the current error amplifier using a PWM comparator, and its output is given to the switch. In this technique, the current being measured through the inductor is the average current rather than the peak current so that it can follow the supply voltage [26,27]. In applications involving power factor enhancement that use average current mode control, the converter runs at its greatest percentage of duty ratio during the crossing of zero of the supply voltage. Because this zero crossing represents the point where the supply voltage reaches zero.
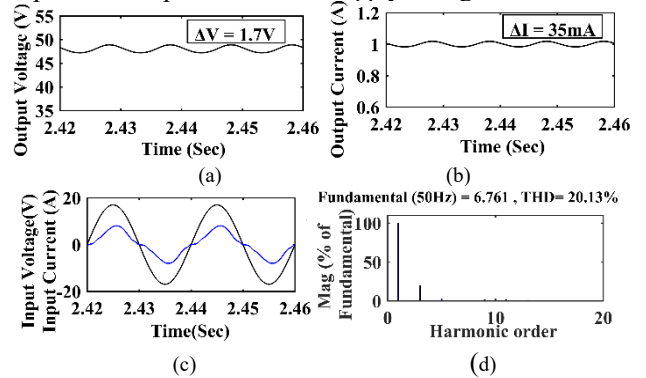


(a)

(b)

(c)

(d)

Fig. 5 – Simulated waveform of average current control loop boost-flyback integrated converter (a) Output voltage at constant load (b) output current at constant load (c) Supply voltage and current at constant load (d) Input current THD spectrum.

The main drawbacks are the need to detect the inductor current, the error voltage amplifier, and the compensator circuit setup. To optimize the line period, all these aspects

must be carefully considered across the converter's different operating points.

Figure 5 shows the simulated waveform of resultant voltage, resultant current, supply voltage, supply current, and THD spectrum for the average current control boost-flyback converter at constant load. The THD is 20.13 %.

## 3.2 CURRENT PROGRAMMED MODE CONTROL TECHNIQUE

The switching cycle starts by giving a clock pulse to the set input of the SR-flip flop, which makes the resultant of the SR-flip flop set a high value. This, in turn, causes the switch to be switched on. The switch current and inductor current become identical once switched on, which results in an upward inclination of this current depending upon the inductance's value and converter voltage. Over time, the switch current and the control signal will converge, so the inductor current will begin to decrease. Figure 6 exhibits the switch current and control input waveform current programmed mode switch technique.
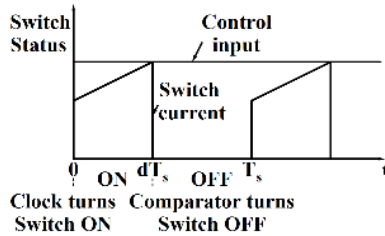
Fig. 6 – Switch current and control input of current programmed mode switch technique.

The voltage appropriate to the switch current and the control input is balanced in actual operation by an equality constant known as $R_f$. The comparator will let go of the latch and toggle the switch OFF for the rest of the switching time once the switching current has been adequate to attain the control input. The drawback of using current programmed mode control is that it is easily susceptible to noise. The noise could result in the latch being reset too soon, disrupting the controller's normal functionality. The issue of subharmonic oscillation affects the current programmed mode control when the duty cycle is higher than fifty percent. Including a simulated ramp signal will rectify the switch current being measured.
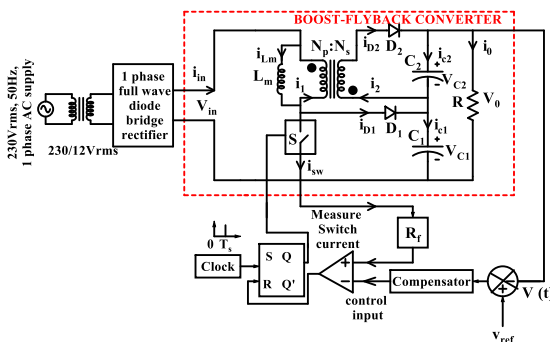
Fig. 7 – Current programmed mode control boost-flyback integrated converter.

Figure. 8(a-d) shows the simulated waveform of resultant voltage, resultant current, supply voltage, supply current, and THD spectrum current programmed mode control boost-flyback converter at rated load. The THD is 8.19 %.
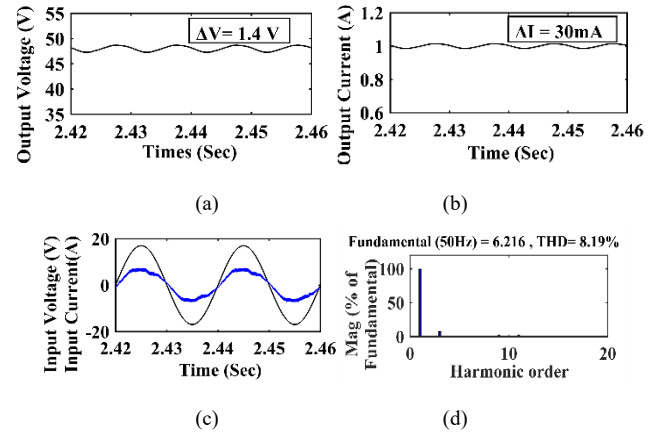
Fig. 8 – Simulated waveform of current programmed mode control loop boost-flyback integrated converter: (a) output voltage waveform at constant load; (b) output current waveform at constant load; (c) input voltage and current waveform at constant load, (d) input current THD spectrum.

## 4. PROPOSED CURRENT SENSORLESS CONTROL TECNHIQUE

Control of boost flyback integrated ac/dc PFC converter without the need for current sensors is presented in this work as a novel technique. Numerous PFC control algorithms make use of the existing sensorless methodology. Supplying an ac source for light-emitting diode (LED) lighting, the suggested sensorless control technique does not rely on a current sensor to generate a power factor of one. It generates a power factor (PF) of approximately one, a current with a sinusoidal waveform, a relatively small level of harmonics in the source current, and a rapid response to change during transient operation.

For the PFC technique, normally, the input current and input voltage are sensed. It is a complicated problem to detect the input current. The three most popular sensors are capacitive, inductive, and resistive. Of the three, resistive sensors are the most widely used but also the most difficult and expensive to utilize since they generate heat and power losses. There are numerous PFC control methods in the present sensorless methodology. Simulation and hardware results show the proposed control mechanism's efficacy and viability.
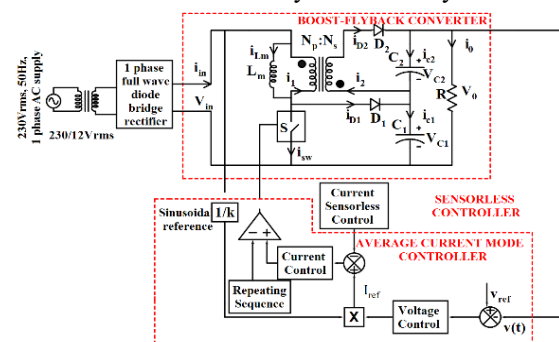
Fig. 9 – Current sensorless control Boost-flyback integrated converter.

There are two different states for the boost-flyback integrated converter. The predicted inductor current is expressed as follows when the switch is on:

$$V_{in}=L_m\frac{di_{Lm}}{dt}, \qquad (21)$$

$$i_{Lm}=\frac{V_{in}}{L_m}t_{on}. \tag{22}$$

The anticipated inductor voltage is stated as,

$$V_{Lm}=V_{in}-V_{C1}, \tag{23}$$

$$i_{Lm}=\frac{V_{in}-V_{C1}}{L_m}t_{off}. \tag{24}$$

Therefore, total iLm is give as,

$$i_{Lm}=\frac{2V_{in}D}{L_m f}. \tag{25}$$

The proposed control method's schematic diagram without a current sensor is depicted in Fig. 10.
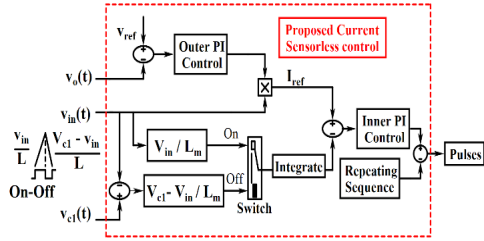


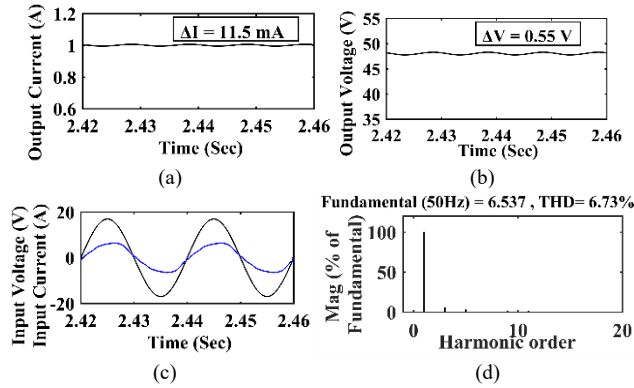Fig. 10 – Proposed control strategy without a current sensor.



Fig. 11 – Simulated waveform of current sensorless control loop boost-flyback integrated converter: (a) output voltage waveform at constant load; (b) output current waveform at constant load; (c) input voltage and current waveform at constant load, (d) input current THD spectrum.

Figure 11 shows the simulated waveform of resultant voltage, resultant current, supply voltage, supply current and THD spectrum of current sensorless boost-flyback converter at rated load. The THD is 6.73 %.

*Table 2*

Simulated comparison of boost-flyback integrated converter

| Paramaters | Supply PF | THD (%) | Distortion factor | Efficiency (%) | $\Delta V_0$ (V) | $\Delta I_0$ (mA) |
|---|---|---|---|---|---|---|
| Boost-flyback Integrated converter | 0.978 | 26.59 | 0.754 | 87.30 | 2 | 40 |
| Average control technique | 0.998 | 20.13 | 0.915 | 89.25 | 1.7 | 35 |
| Current control technique | 0.998 | 8.19 | 0.971 | 89.08 | 1.4 | 30 |
| Sensorless control technique | 0.999 | 6.73 | 0.978 | 89.48 | 0.55 | 11.5 |

## 5. EXPERIMENTAL RESULTS

A hardware model of ba boost-flyback integrated converter in an open loop and closed loop using a sensorless controller is evaluated, and the outcomes are

reported to validate the results of the simulation. Figure12 displays the boost-flyback integrated converter. An FPGA controller is used to create the suggested converter's gating pattern. The driver can power a 48 W load operating at a voltage range of 12 $V_{rms}$. An output voltage of 48 V and an output current of 1A are required to drive the load. The proposed converters' results are recorded using a digital signal oscilloscope (DSO) MY57152389.
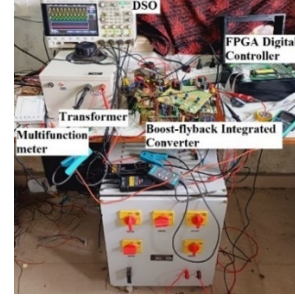


Fig. 12 – Hardware setup of Boost-flyback integrated converter.

The hardware output voltage ripple $\Delta V_o$ = 0.5 V, $\Delta I_o$ = 12 mA of current ripple, is much less than that of other controllers. The THD is 6.5 %. To determine the THD and PF of the suggested converter, a multifunction meter is employed to measure alternating current parameters. The power factor is 0.991. The boost flyback converter efficiency was calculated to be 89.02 %.
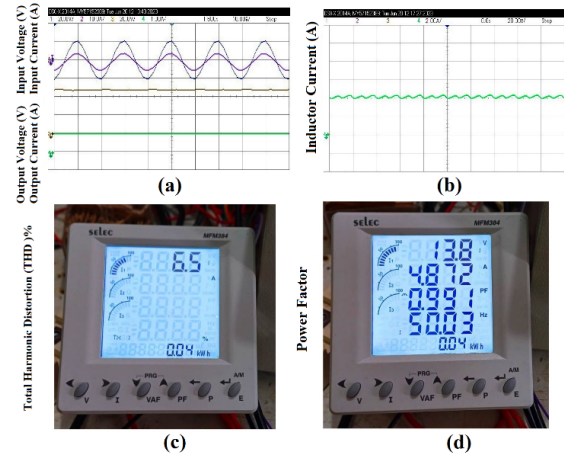


Fig. 13 (a-d) –Hardware results of boost-flyback integrated converter for rated load using sensorless controller.

*Table 3*

Simulated and Hardware comparison of Boost-flyback converter.

| Parameters | Simulated values | Hardware values |
|---|---|---|
| Input current THD | 6.73 % | 6.5 % |
| Input power factor | 0.999 | 0.991 |
| Output ripple voltage | 0.55 V | 1 V |
| Output ripple current | 11.5 mA | 25 mA |
| Percentage of output ripple voltage (%ΔV) | 1.145 % | 2.08 % |
| Percentage of output ripple current (%ΔI) | 1.24 % | 2.5 % |
| Efficiency (%) | 89.48 % | 89.02 % |

## 6. CONCLUSIONS

To improvise the waveshape of the input current, various current control techniques were simulated, and a comparative analysis was done. An innovative control method for LED drivers that produces high PF and does away with current sensors is provided in this work. This method circumvents the issues that arise when utilizing a current sensor by being straightforward and dependable in

estimating inductor current. The voltage across the inductor during switch on and off determines the inductor current. Simulation outcomes are offered to demonstrate the viability of the proposed scheme. A 48 W experimental prototype model has been built and tested to evaluate the boost-flyback integrated circuit. The hardware results demonstrate that the proposed technique exhibits a sinusoidal input current waveform with an impressively low total harmonic distortion (THD) of 6.5 %. Furthermore, the power factor (PF) is measured to be 0.991, indicating a high-efficiency level and a close alignment between the voltage and current waveforms. The output voltage ripple is 2.08 %, and the current ripple is 2.5 %. With the aid of hardware results, the simulation results are verified. The proposed converter with sensorless techniques results in less ripple and a prolonged lifespan for the LED lighting application.

## REFERENCES

1. V.K. Yadav, A.K. Verma, U.R. Yaragatti, *High PFC integrated stage single switch ac-dc system for LED power driver*, International Conference on Sustainable Energy and Future Electric Transportation, pp. 1–6 (2021).
2. \*\*\* EN61000-3-2 - *Limits for harmonic current emissions (equipment input current up to and including 16A per phase)*, 30th European Committee for Electrotechnical Standardization, Belgium, (2014).
3. W.Y. Choi, J.M. Kwon, B.H. Kwon, *Efficient LED back-light power supply for liquid-crystal-display*, IET Electric Power Application, **1**, *2*, pp. 133–142 (2007).
4. C.C. Raicu, G.C. Seritan, B. Enache, *48 V network adoption for automotive lighting systems,* Rev. Roum. Sci. Techn. – Électrotechn. Et Énerg, **66**, *4*, pp. 231–236 (2021).
5. H. Ma, Y.Li, Q. Chen, L. Zhang, J. Xu, *A single-stage integrated boost-llc ac–dc converter with quasi-constant bus voltage for multichannel LED street-lighting applications*, IEEE Journal of Emerging and Selected Topics in Power Electronics, **6**, *3*, pp. 1143–1153 (2018).
6. C. Cheng, H. Wu, *A novel single-stage high-power-factor ac-dc LED power supply for streetlight applications*, IEEE 7th Global Conference on Consumer Electronics (GCCE), pp. 128–129 (2018).
7. W.Y.Choi, J.M.Kwon, B.H. Kwon *Bridgeless dual-boost rectifier with reduced diode reverse-recovery problems for power-factor correction*, IET Power Electron., **1**, *2*, pp. 194–202 (2008).
8. L. Rossetto, G. Spiazzi G., Tenti P., *Control techniques for power factor correction converters*, Proc. Power Electronics Motion Control, pp. 1310–1318 (1994).
9. K.Rustom, I. Batarseh, *Recent advances in single-stage power factor correction*, IEEE Int. Conf. on Industrial Technology, **2**, pp. 1089–1095 (2003).
10. R. Redl, L. Balogh, *Design considerations for single-stage isolated power-factor-corrected power supplies with fast regulation of the output voltage*, IEEE Applied Power Electronics Conference and Exposition, USA, **1**, pp. 454-458 (1995).
11. R. Munuswamy, U. Govindarajan, K.A. Anbukumar, *Performance comparison and stability analysis of ACM and ENLC controlled SEPIC PFC converter*, IET Power Electronics, **13**, *5*, pp. 991–1001, (2020).
12. K.A. Kumar, V.K.S. Veeramallu, B.L. Narasimharaju, *Performance analysis of coupled inductor-based ripple free boost PFC ac-dc LED driver*, IEEE International Conference on Power Electronics, Drives and Energy Systems, pp. 1–4 (2020).
13. K. Jirasereeamornkul, Y. Roungraungpalangkul, K. Chammongthai, *A single stage single switch power factor correction converter*, ISCAS, **2**, pp. 397–400 (2001).
14. D. Ziane, A. Azib, A. Oubelaid, N. Taib, T. Rekioua, D. Rekioua, *Proposed power factor correction circuit based on the single-ended primary-inductor converter controlled by sliding mode control strategy used in an electric vehicle charging station*, Rev. Roum. Sci. Techn. – Électrotechn. Et Énerg., **67**, *3*, pp. 241–245 (2022).
15. M. Arias, V. Aitor, J. Sebastián, *An overview of the ac-dc and dc-dc converters for LED lighting applications*, Automatika–Journal for Control, Measurement, Electronics, Computing and Communications, **53**, *2*, 156–172 (2012).
16. J.I. Baek, J.K. Kim, J.B. Lee, M.H. Park, G.W. Moon, *A New standby structure integrated with boost PFC converter for server power supply*, IEEE Transactions on Power Electronics, **34**, *6*, pp. 5283–5293 (2019).
17. M.A. Dalla Costa, J.M. Alonso, J.C. Miranda, J. Garcia, D.G. Lamar, *A single-stage high-power-factor electronic ballast based on integrated buck flyback converter to supply metal halide lamps*, IEEE Transactions on Industrial Electronics, **55**, *3*, pp. 1112–1122 (2008).
18. X. Xie, J. Li, K. Peng, C. Zhao, Q. Lu, *Study on the single-stage forward-flyback PFC converter with QR control*, IEEE Transactions on Power Electronics, **31**, *1*, pp. 430-442 (2016).
19. S. Jain, *Comparative study of open loop and closed loop of three-phase active power factor correction based buck converter*, Electrical and Electronics Engineering: An International Journal (ELELIJ), **4**, *1*, pp. 79-86 (2015).
20. J. Park, D.J. Kim, K. Lee, *Predictive control algorithm including conduction-mode detection for PFC converter*, IEEE Transactions on Industrial Electronics, **63**, *9*, pp. 5900–5911 (2016).
21. H.S. Nair, N. Lakshminarasamma, *A computationally simple predictive CCM average current controller with nearly zero tracking error for boost PFC converter*, IEEE Transactions on Industry Applications, pp. 5083-5094 (2020).
22. Z.Y. Chen; Q. Zhou, J. Xu, *Coupled-inductor boost integrated flyback converter with high-voltage gain and ripple free input current*, IET Power Electronics, **8**, *2*, pp. 213–220 (2015).
23. L. Rossetto, G.G. Spiazzi, P. Tenti, *Control techniques for power factor correction converter*, International Conference on Power Electronics and Motion, Control, pp 1310–1318 (1994).
24. C. Zhou, M. Jovanovic, *Design trade-offs in continuous current-mode controlled power-factor correction circuits*, HFPC Conf. Proc., pp. 209–220 (1992).
25. S. Makkapati, S. Ramalingam, *Design and implementation of single stage SEPIC integrated parallel ripple cancellation Method for LED lighting*, Advances in Electrical and Computer Engineering, **22**, *4*, pp. 39–46 (2022)
26. B. Lekshmi Sree, M.G. Umamaheswari. *A Hankel matrix reduced order SEPIC model for simplified voltage control optimization and MPPT*, Solar Energy, **170**, pp. 280–292 (2018).
27. A. Sangari, R. Umamaheswari, M.G Umamaheswari, B. Lekshmi Sree, *A novel SOSMC based SVPWM control of Z-source inverter for ac microgrid applications*, Microprocessors and Microsystems, **75**, 103045 (2020).